ACS APPLIED MATERIALS & INTERFACES

Research Article

www.acsami.org

Fabrication of Elemental Copper by Intense Pulsed Light Processing of a Copper Nitrate Hydroxide Ink

Gabriel L. Draper,[†,‡] Ruvini Dharmadasa,[‡] Meghan E. Staats,[†] Brandon W. Lavery,[†,‡] and Thad Druffel*[,‡]

[†]Department of Chemical Engineering, J. B. Speed School of Engineering, University of Louisville, Louisville, Kentucky 40292, United States

[‡]Conn Center for Renewable Energy Research, University of Louisville, Louisville, Kentucky 40292, United States

Supporting Information

ABSTRACT: Printed electronics and renewable energy technologies have shown a growing demand for scalable copper and copper precursor inks. An alternative copper precursor ink of copper nitrate hydroxide, $Cu_2(OH)_3NO_3$, was aqueously synthesized under ambient conditions with copper nitrate and potassium hydroxide reagents. Films were deposited by screen-printing and subsequently processed with intense pulsed light. The $Cu_2(OH)_3NO_3$ quickly transformed in less than 100 s using 40 (2 ms, 12.8 J cm^{-2}) pulses into CuO. At higher energy densities, the sintering improved the bulk film quality. The direct formation of Cu from the $Cu_2(OH)_3NO_3$ requires a reducing agent; therefore, fructose and glucose were added to the inks. Rather than oxidizing, the thermal decomposition of the sugars led to a reducing environment and direct conversion of the films into elemental copper. The chemical and physical transformations were studied with XRD, SEM, FTIR and UV−vis.

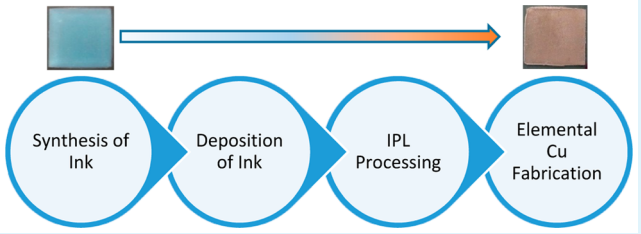

KEYWORDS: *copper, conductivity, intense pulsed light, nanoparticle synthesis, reduction, copper nitrate hydroxide*

INTRODUCTION

The deposition of conductive metal traces for electronics onto various substrates is typically accomplished through physical, vapor, and electrodeposition routes. These techniques have gained widespread acceptance in a number of applications in electronics. Recently, there has been interest in depositing these conductive patterns utilizing more versatile techniques such as screen, inkjet and aerosol jet printing. These approaches allow for on demand customization of the patterns as well as more affordable substrates, which can vastly reduce the costs of a number of important devices such as RFID, solar cells, flexible electronics and displays.

Inks used for the printing of conductive traces are typically composed of metal particles, binders and emulsifiers suspended in a solvent. Silver has been the metal of choice for most of these applications, but copper has begun to gain a fair amount of interest primarily because the cost is substantially lower. The deposited inks are then processed by heat that both removes the remaining organics and sinters the particles producing a conductive trace. Recently, intense pulsed light (IPL) has been utilized as a rapid and scalable technique to accomplish the heat treatment. IPL is an emerging advanced manufacturing process that illuminates light from a xenon strobe over a wide area, which locally heats a film. The IPL process is particularly advantageous as an alternative method of sintering metal nanoparticles, as the rapid pulses would significantly reduce processing times[1] and is applicable to flexible substrates, which would be irreversibly damaged by traditional thermal sintering.[2] Utilizing inks with metal particles in the nanosize range decreases the required sintering temperature, due to the increased surface to volume ratio of the particle, resulting in the particles having a low melting point temperature. This phenomenon has been reported for a number of nanoparticles, including gold[3] and copper.[4]

IPL processing of copper nanoparticles has enabled the sintering of copper, without the use of an inert environment or vacuum because the time frame of heating and cooling is faster than the oxidation of the copper.[5] Forgoing the use of inert environments and vacuum processes is enticing for scaled manufacture due to the associated costs. IPL sintered copper nanoparticles have shown very good conductivities[1] and sintering/melting at 318 °C.[6] However, the solution stabilized copper nanoparticles were susceptible to oxidation and agglomeration. To counter oxidation, the synthesis/deposition of copper nanoparticles used harsh reducing agents of hydrazine[7] and sodium borohydride.[8,9] Additives such as PVP[10] or CTAB[11] can increase the solution stability and control the particle size of the copper nanoparticles, but there is an inherent trade-off when adding large molecules and polymers on the resulting porosity/conductivity of IPL processed films.[12] To overcome the agglomeration and oxidation challenges of copper during synthesis and deposition, it is advantageous to use cuprous oxide[8] and cupric oxide.[13] Reducing the oxides after printing has been accomplished as the

Received: May 4, 2015
Accepted: July 8, 2015
Published: July 8, 2015

DOI: 10.1021/acsami.5b03854
ACS Appl. Mater. Interfaces 2015, 7, 16478−16485

IPL process can induce a reducing environment by the thermal decomposition of organic molecules (Table 1).

Table 1. Select Examples of Copper Precursors Used with Organic Molecules that Decompose during IPL Processing

material	organics	heating mechanism
Cu (native Cu_2O shell)	PVP	IPL[4]
Cu_2O	methanol, ethanol, isopropyl alcohol, *tert*-butanol, butylaldehyde, acetone, formic acid, acetic acid, and hydrogen	thermal[27]
Cu_2O	tergitol and ethylene glycol	IPL[8]
Cu_2O@NiO	tergitol and ethylene glycol	IPL[30]
copper formate, $Cu(HCOO)_2$	metal−organic copper complex	IPL[21]
copper acetate, $Cu(CH_3COO)_2$		
copper oleate, $Cu(C_{17}H_{33}COO)_2$		

Alternatively, the dispersion stability of copper hydroxides is even greater than that of copper oxides[14] though the copper hydroxides are typically utilized as precursors/templates for nanowires[15−17] due to their low thermal stability of 236−280 °C (copper nitrate hydroxide)[18] and 400 °C (copper hydroxide).[19] However, these relatively low temperatures become enticing for printed electronics if the hydroxides can be reduced into elemental copper.

In this work, a synthesis for copper nitrate hydroxide has been developed to aid in the solution stability of an ink and to enhance the transformation into bulk copper with the IPL process. A simple room temperature aqueous synthesis was implemented, employing a copper salt and potassium hydroxide reagents, forming copper nitrate hydroxide as an alternative low cost copper precursor ink. Through the IPL process, copper nitrate hydroxide was successfully converted into cupric oxide (CuO). With the introduction of organic molecules, which thermally decompose below 200 °C however, copper nitrate hydroxide was converted into conductive copper. Fructose and glucose were the chosen organic molecules studied, as they are readily available chemicals that can increase the viscosity of the inks. In this paper, the mechanisms of the synthesis, transformation, and reduction of copper nitrate hydroxide are thoroughly studied, which will lead to a pathway toward the scalable production of conductive copper thin films.

RESULTS AND DISCUSSION

Process Overview. The overall process is illustrated with Figure 1 and envisioned for future scaled, commercial applications. The $Cu_2(OH)_3NO_3$ is formed through a copper salt and hydroxide salt reaction. Depending on the desired printing method, additives could be added to the dispersion or the $Cu_2(OH)_3NO_3$ could be separated from the water prior to formulation. For example, to formulate a screen printed paste, the $Cu_2(OH)_3NO_3$ precipitate is mixed with the chosen organic, deposited as an additive pattern, and then subsequently IPL processed to create conductive copper.

Synthesized Copper Nitrate Hydroxide. The synthesis was designed to be simple and faster than a copper oxide synthesis while avoiding the addition of large organic molecules, harsh reducing agents and polymers. The synthesis of copper nitrate hydroxide is favorable over the synthesis of copper hydroxide as it provides a lower thermal decomposition temperatures of 236−280 °C (copper nitrate hydroxide)[18] and 400 °C (copper hydroxide).[19] The technique utilizes the dropwise addition of an aqueous potassium hydroxide solution into an aqueous solution of copper salt generating a localized increase in hydroxide ions surrounded by a much larger nitrate ion concentration, leading to the formation of $Cu_2(OH)_3NO_3$

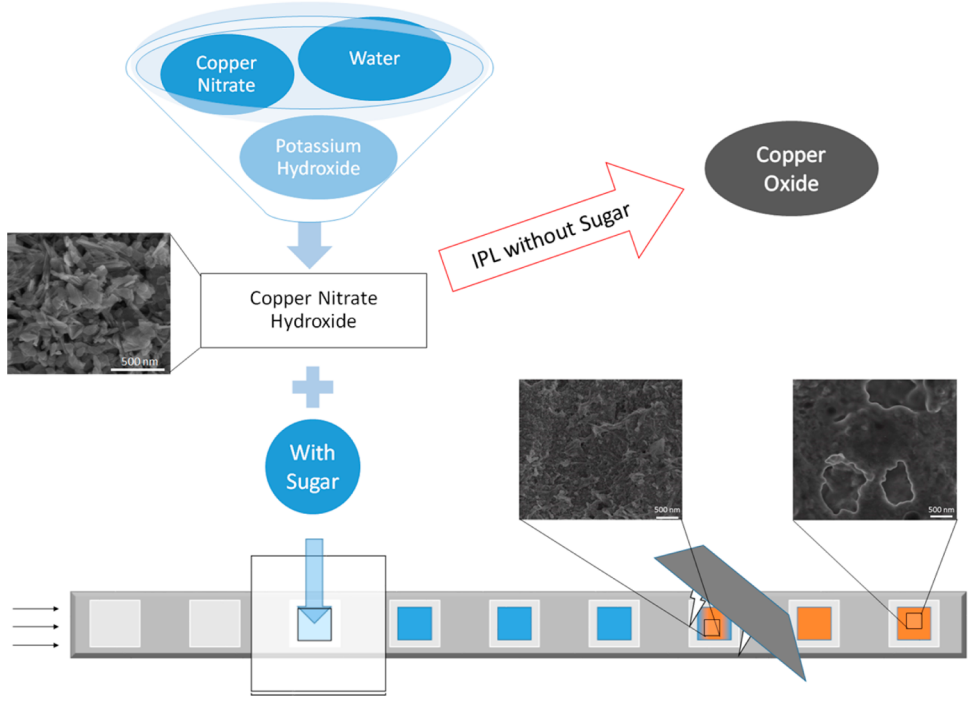

Figure 1. Overview schematic of $Cu_2(OH)_3NO_3$ conversion into conductive copper from synthesis to deposition and IPL processing with SEM images of the respective fructose sample.

DOI: 10.1021/acsami.5b03854
ACS Appl. Mater. Interfaces 2015, 7, 16478−16485

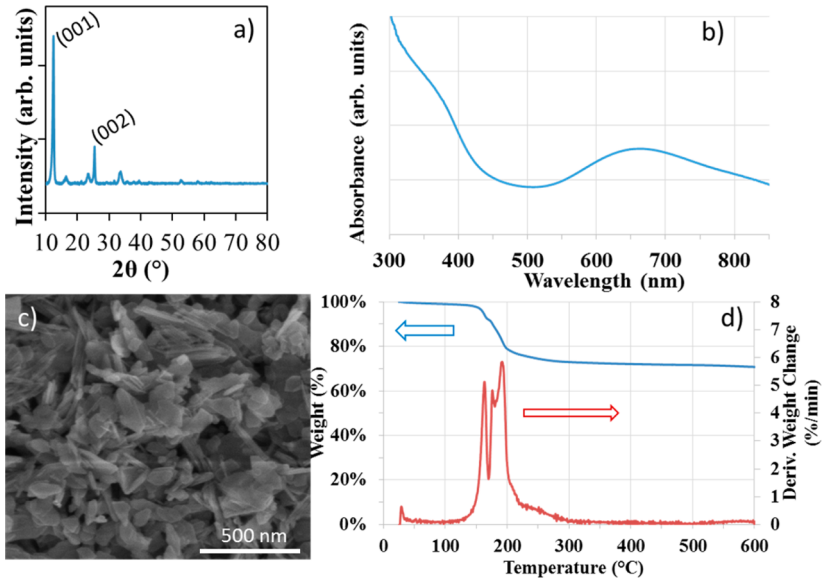

Figure 2. Characterization of synthesized copper nitrate hydroxide: (a) XRD, (b) absorbance, (c) SEM and (d) TGA.

and prevention of $Cu(OH)_2$ formation. The coppers are coordinated through either two OH^- groups or an OH^- group and a NO_3^- group.[20] The reaction proceeds at ambient conditions, with copper(II) nitrate hemipentahydrate ($Cu(NO_3)_2{\cdot}2.5H_2O$) and potassium hydroxide reagents to form the $Cu_2(OH)_3NO_3$ as shown in eq 1.

$$2Cu(NO_3)_{2(aq)} + 3KOH_{(aq)} \leftrightarrow Cu_2(OH)_3NO_{3(s)} + 3KNO_{3(aq)} \quad (1)$$

To confirm the presence of different material phases, X-ray diffraction (XRD) was employed. XRD analysis of the as-synthesized deposits displayed the strongest peak at 2θ = 12.36° (d-spacing of 6.93 Å). There was no apparent peak at 16.7135° (5.30 Å) (ICDD 00-013-0420), eliminating the presence of $Cu(OH)_2$. Although copper hydroxide hydrate's, $Cu(OH)_2{\cdot}H_2O$, peak of 13.3294° (6.637 Å) (ICDD 00-042-0638) was similar, the results aligned more closely with the copper nitrate hydroxide, $Cu_2(OH)_3NO_3$ peak of 12.8045° (6.9078 Å) (ICDD 01-075-1779) (Figure 2a). The presence of copper nitrate hydroxide was also indicated by the UV−vis absorption spectrum as the sample produced a broad peak ranging from approximately 550−850 nm (with a maximum at 650 nm) (Figure 2b). The increase in optical adsorption peak was consistent with the Cu(II) complex findings reported in the literature.[1,21] This increase in optical absorbance is also highly advantageous for the IPL process, which relies on the absorption of visible light to initiate localized heating leading to decomposition and sintering. That enhancement mitigates the decreased absorbance, which would typically be seen when using an alternative precursor as observed with similar copper(II) salt structures.[21]

SEM micrographs of the synthesized $Cu_2(OH)_3NO_3$ showed an assortment of morphologies (spherical, rod, platelet) (Figure 2c). However, optimization to obtain a narrow dispersion of particle size and morphology was not a priority of this work since the focus is the mechanics of the IPL process of $Cu_2(OH)_3NO_3$ to produce a Cu film where the IPL process is intended to modify the morphology of the deposited ink.

Further characterization of the $Cu_2(OH)_3NO_3$ was carried out through thermogravimetric analysis (TGA) (Figure 2d). The first peak at 160 °C is attributed to the weight loss of adsorbed water at approximately 17 wt %, which is similar to the value of 158 °C observed in the literature.[22] The remaining weight change of approximately 30% from 160 to 250 °C represented the thermal decomposition of $Cu_2(OH)_3NO_3$ to CuO which is in agreement with reported values.[23]

Conversion to CuO during IPL. The thermal decomposition was also observed when the $Cu_2(OH)_3NO_3$ was IPL processed without a generated reducing environment. IPL processed films have been shown to rise to high temperatures 300 °C at an energy density of 8.3 J cm^{-2} and 500 °C at an energy density of 17.6 J cm^{-2} for CdS.[24] $Cu_2(OH)_3NO_3$'s thermal decomposition values of 236−280 °C[18] were well within these temperature ranges and the thermal decomposition reaction of $Cu_2(OH)_3NO_3$ can be represented by eq 2. At temperatures higher than 250 °C, however, HNO_3 converts to NO_2, H_2O and O_2.[25] The formation reaction of cupric oxide would then be represented as eq 3.[23]

$$Cu_2(OH)_3NO_{3(s)} \rightarrow 2CuO_{(s)} + HNO_{3(g)} + H_2O_{(q)} \quad (2)$$

$$4Cu_2(OH)_3NO_{3(s)} \rightarrow 8CuO_{(s)} + 4NO_{2(g)} + 6H_2O_{(g)} + O_{2(g)} \quad (3)$$

The as-synthesized $Cu_2(OH)_3NO_3$ was deposited as a film then subsequently processed using the IPL process, which induced a localized rise in temperature. This increase in temperature is high enough to both desorb water and convert the $Cu_2(OH)_3NO_3$ to CuO. The initial pulses are used to remove the adsorbed water, which occurs within the first five and 10 pulses as shown in Figure S1 of the Supporting Information. Following water desorption, the $Cu_2(OH)_3NO_3$ begins to undergo conversion as described by eqs 2 and 3.

The samples visually changed from a pale blue to black as the process proceeded, which serves as a visual indicator of the transformation of $Cu_2(OH)_3NO_3$ to CuO. The $Cu_2(OH)_3NO_3$ transformation into CuO throughout the IPL process was monitored using XRD analysis (Figure 3a). The IPL processed

DOI: 10.1021/acsami.5b03854
ACS Appl. Mater. Interfaces 2015, 7, 16478−16485

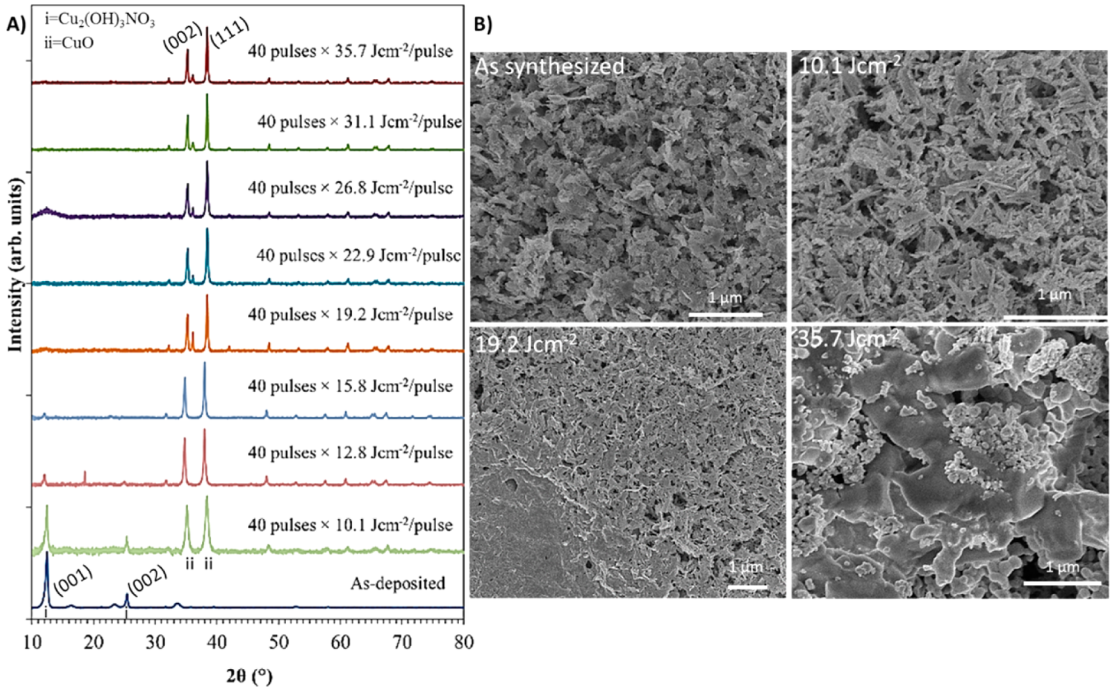

Figure 3. (A) XRD results with IPL processing of 40 pulses at increasing energy densities. (B) SEM images of IPL processed copper nitrate hydroxide films with 40 pulses at varying energy densities.

at an energy density of 10.1 J cm^{-2} showed significant change in the crystal lattice to CuO. At an energy density of 12.8 J cm^{-2}, at similar pulse number and rate, only trace amounts of $Cu_2(OH)_3NO_3$ were present. At 19.2 J cm^{-2}, the $Cu_2(OH)_3NO_3$ peaks are no longer present. At higher energy densities than 19.2 J cm^{-2}, there is little variation in the crystal structure.

The resulting CuO films displayed significant sintering and melting with increasing energy density as shown in the SEM micrographs (Figure 3). Little to no changes were observed to the sintering with the application of 40 10.1 J cm^{-2} pulses, though partial conversion to CuO were observed in the XRD (Figure 3b). At an energy density of 19.2 J cm^{-2} (Figure 3c), significant sintering was observed and, in certain areas of the film, melting. Furthermore, at an energy density of 35.7 J cm^{-2}, vast areas of melting of the CuO are observed.

Copper Conversion. The aim of this study was to investigate the potential for $Cu_2(OH)_3NO_3$ as an alternative precursor for conductive copper that requires conversion to elemental copper. According to eqs 2 and 3, the direct conversion to of $Cu_2(OH)_3NO_3$ to elemental Cu was not expected nor was it observed. However, it has been shown previously that conversion of CuO and Cu_2O during the IPL process to Cu can be achieved through the addition of reducing agents (Table 1). The direct conversion of $Cu_2(OH)_3NO_3$ can also be accomplished in the presence of a hydrogen atmosphere as modeled by eq 4.

$$Cu_2(OH)_3NO_3 + 2H_2 \rightarrow 2Cu + 3H_2O + HNO_3 \quad (4)$$

Four hydrogen atoms in total are needed to isolate the copper atoms. The hydrogen atoms integrate with the nitrate group and three hydroxyl groups to transform to form nitric acid and water, respectively.

The previous section showed that the oxidation of $Cu_2(OH)_3NO_3$ occurred rapidly with CuO emerging at an energy density of 10.1 J cm^{-2}, which was the lowest energy density used in this work. Therefore, the most efficient formation of copper requires that the reducing environment be induced prior to significant transformation of $Cu_2(OH)_3NO_3$ to CuO. The direct conversion of $Cu_2(OH)_3NO_3$ to Cu would be favorable, as it would decrease the energy needed for conversion when compared to energy to convert into CuO and then reduce CuO into Cu. A reducing environment can be established through the decomposition of organic molecules (Table 1). Therefore, it would be desirable to utilize organic molecules, which are abundant and cost efficient, and environmentally friendly. These criteria are met by both fructose and glucose.

An analogous atomic representation of the overall transformation of $Cu_2(OH)_3NO_3$ with fructose or glucose leads to eq 5, as both fructose and glucose have the same atomic structure (though differ in their molecular structure which leads to varying material properties). According to eq 5, the molar ratio of $Cu_2(OH)_3NO_3$ to monosaccharide is 18:1, setting the minimum amount of monosaccharide at 3.18 wt % to $Cu_2(OH)_3NO_3$. A 10 wt % monosaccharide concentration was used due to the high viscosity printing requirements, which is more than sufficient to create the reducing atmosphere upon decomposition. The decomposition leads further into smaller organic molecules throughout the process. One of the main decomposition products is formic acid.[26] The reduction reaction for $Cu_2(OH)_3NO_3$ can be represented as eq 6. Equation 6 is similar to a Cu_2O reduction mechanism from the literature.[27]

$$18Cu_2(OH)_3NO_3 + C_6H_{12}O_6 \rightarrow 36Cu + 6CO_2 + 24H_2O + 18HNO_3 \quad (5)$$

$$Cu_2(OH)_3NO_3 + 2HCOOH \rightarrow 2Cu + 2CO_2 + 3H_2O + HNO_3 \quad (6)$$

DOI: 10.1021/acsami.5b03854
ACS Appl. Mater. Interfaces 2015, 7, 16478−16485

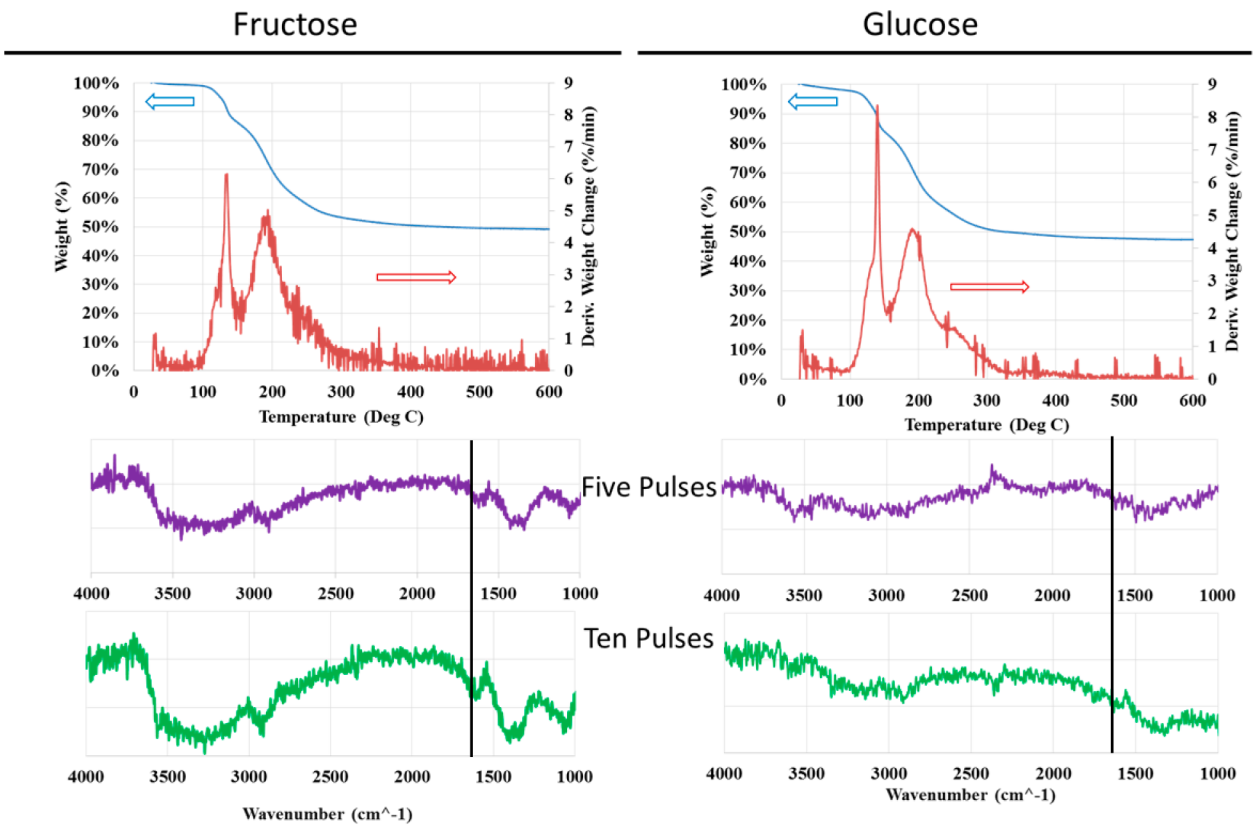

Figure 4. TGA and then the FTIR 12.8 J cm^{-2} IPL processed fructose (left) and glucose samples (right).

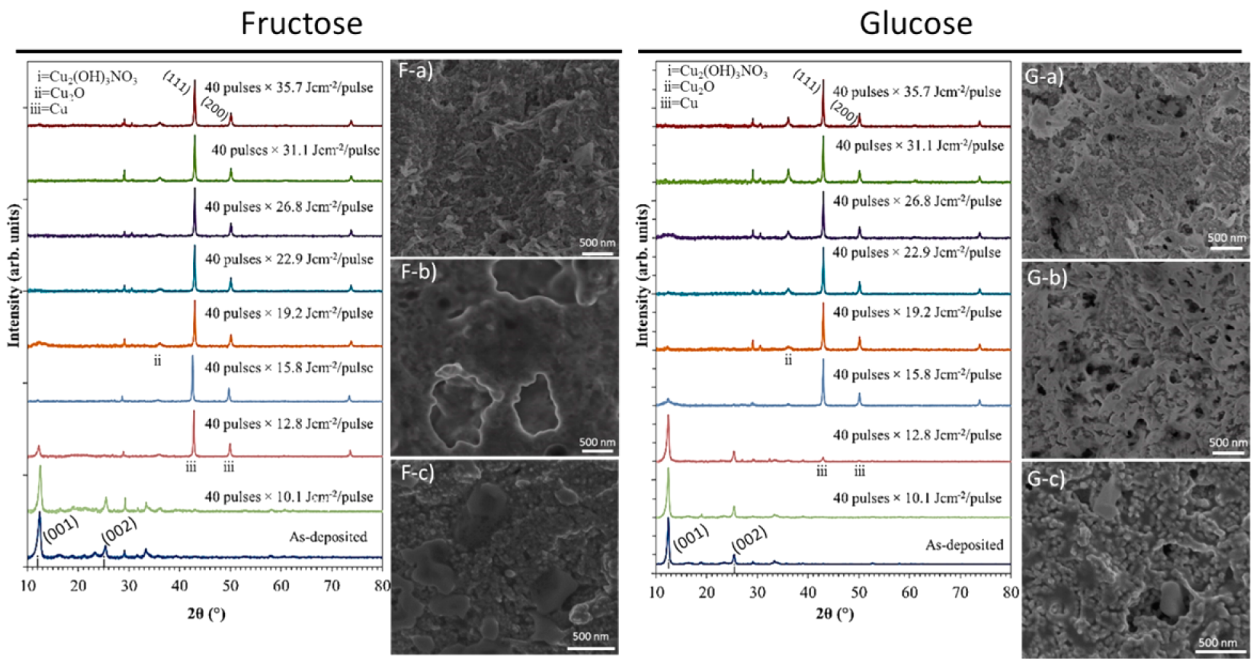

Figure 5. XRD results with IPL processing of 40 pulses at increasing energy densities for fructose (left) and glucose (right). SEM images of fructose (F-a,b,c) and glucose (G-a,b,c) samples at different energy densities of IPL processing (a) 12.8 J cm^{-2}, (b) 15.8 J cm^{-2} and (c) 35.7 J cm^{-2}.

The most important differences between fructose and glucose for this study were the thermal decomposition temperature, enthalpy of decomposition, and resulting by-products. Thermogravimetric analysis (TGA) helped to identify how these differences affect the $Cu_2(OH)_3NO_3$ reduction (Figure 4). During the TGA analysis, both the fructose and glucose samples displayed a similar behavior or weight change throughout the 150 to 220 °C range. The fructose sample had an additional weight change from 100 to 120 °C followed by a more rapid weight change from 125 to 145 °C. The largest peak is attributed to fructose in 125 to 145 °C range. The glucose sample had very similar peaks though the peak was

DOI: 10.1021/acsami.5b03854
ACS Appl. Mater. Interfaces 2015, 7, 16478−16485

observed at 175 °C compared to 145 °C for the fructose sample. The observed temperature difference of approximately 30 °C is comparable to literature value differences of the thermal decomposition temperatures with 138.7 °C (fructose) and 166.4 °C (glucose) resulting in a 27.7 °C difference.[28] The reported values are higher than the literature values as the thermal decomposition temperatures are known to vary with the heating rate.[28] The observed weight losses (53% for fructose and 55% for the glucose) were larger than the 30% weight loss during conversion to CuO. The increased weight loss was anticipated as the transformation of $Cu_2(OH)_3NO_3$ to CuO versus Cu differs with an oxygen atom, the weight loss associated with the decomposition of fructose and glucose, and varying water contents in the samples.

Fructose is known to decompose thermally (ΔH_{rxn} = 11.09 kcal/mol) into glyceraldehyde and 1,3-dihydroxyacetone whereas glucose (ΔH_{rxn} = 12.06 kcal/mol) decomposes into erythrose and glycolaldehyde.[29] To confirm the formation of decomposition products by observing aldehyde and carboxylic groups, specific FTIR was performed with lower IPL processing than used anywhere else in the study with only five and ten pulses at an energy density of 12.8 J cm^{-2} being applied. FTIR analysis primarily displayed peaks characteristic of fructose and glucose with O−H bonds (3500−3200 cm^{-1}) and C−C alkane bonds (3000−2800 cm^{-1}). With five and ten 12.8 J cm^{-2} IPL pulses, the formation of characteristic bonds for the fructose and glucose decomposition, such as aldehyde and carboxylic acid groups (1750−1650 cm^{-1}), began to emerge. The $Cu_2(OH)_3NO_3$ peaks of bonded O−H, $Cu_2(OH)_3NO_3$ (1421, 1047 cm^{-1}, N−O bonds (1384 and 872 cm^{-1}) also became more readily observed (Figure 4). The observed O−H bonds peaks showed a decreasing trend and an emergence of new peaks within the 1750−1650 cm^{-1} range. These peaks are characteristic of functional groups containing double bonded oxygen molecules (aldehydes and carboxylic acids). The presence of these peaks, at a relatively low total energy input of this study, suggests that the decomposition is happening prior to the conversion of copper hydroxide nitrate and leading toward a reducing environment.

The conversion to Cu happened at an IPL energy density of 12.8 J cm^{-2} for fructose and 15.8 J cm^{-2} for glucose as shown with XRD in Figure 5 as the strongest XRD peaks became 43.472 (111), 50.373 (200) and 73.995, which are consistent with the crystalline structure of Cu (ICDD 00-001-1241). The XRD analysis did not show a significant presence of either Cu_2O or CuO during the IPL reduction process. Trace signs of Cu_2O can be seen in the XRD though they are associated with copper's exposure to oxygen/water in the atmosphere.

Higher IPL energy densities were studied to characterize the sintering of the formed films. Because the fructose samples had an earlier conversion to Cu, a higher degree of sintering was observed in the fructose samples (Figure 5F-a,b,c) when compared to the glucose samples (Figure 5G-a,b,c) at the same energy density. At an energy density of 12.8 J cm^{-2}, SEM images of the fructose sample (Figure 5F-a) and glucose samples (Figure 5G-a) begin to show a slightly higher porosity than the deposited films as the organic molecule decomposition leads to gas evolution and disruption of the films. At an energy density of 15.8 J cm^{-2}, the fructose sample (Figure 5F-b) show a higher degree of sintering and melting toward a bulk film whereas the glucose samples (Figure 5G-b) only have particle necking present and still maintain a resemblance to the deposited films. At an energy density of 35.7 J cm^{-2}, both the fructose sample (Figure 5F-c) and glucose samples (Figure 5G-c) have a lower degree of porosity as the IPL processing provides the energy to sinter the Cu films.

Sheet Resistance. As the fructose samples displayed the preferable results with an earlier onset of copper nitrate hydroxide converting into copper, the sheet resistance for these samples were measured throughout the IPL process (Figure S3 of the Supporting Information). The sheet resistance of the films continued to decrease as the intensity of the pulse was increased with a sheet resistance of 0.224 Ω/□ at 35.7 J cm^{-2}. The bulk resistivity of the films can be found by the product of the sheet resistance and the film thickness (ρ = tRs), incorporating a thickness of 5.59 μm, the bulk resistivity for the 35.7 J cm^{-2} sample is $1.251 \cdot 10^{-4}$ Ω·cm; within two magnitudes of bulk copper's resistivity. The resistivity was higher than that of bulk copper, which can be attributed to the porosity of the deposited films. Porosity of the films was caused by the volume change going from $Cu_2(OH)_3NO_3$ to Cu and organic decomposition reactions leading to gas evolution.

EXPERIMENTAL SECTION

Synthesis. The copper nitrate hydroxide was synthesized by the reaction of copper nitrate and potassium hydroxide eq 1. Copper nitrate hydrate $Cu(NO_3)_2 \cdot 2.5H_2O$, Alfa Aesar, 99.99%) was purchased from Alfa Aesar. Potassium hydroxide pellets (KOH, 98%) were purchased from Sigma-Aldrich. Twenty-four grams (0.103 mol) of $Cu(NO_3)_2 \cdot 2.5H_2O$ was dissolved in 200 mL of deionized water. In a separate beaker was dissolved 11.64 g (0.207 mol, 4.16 M) of KOH in 100 mL of deionized water. The $Cu(NO_3)_2$ solution was stirred using a magnetic stirrer and the KOH solution was added to the solution at a rate of 1.67 mL/min^{-1} using a syringe pump. After all of the KOH was added to the solution, the mixture was then placed in an ultrasonic bath for 30 min. The pale light blue precipitate was isolated by centrifuging the mixture at 7000 rpm for 3 min. The precipitate was washed once with deionized water.

Deposition. For deposition, 10 wt % monosaccharide was chosen to control the reducing atmosphere during the IPL process from decomposition and to increase the viscosity of the inks for screen printing. Inks were prepared by fructose or glucose with copper nitrate hydroxide through mixing 10 g (90 wt %) of $Cu_2(OH)_3NO_3$ with 1.01 g (10 wt %) of monosaccharide (fructose or glucose) with a mortar and pestle prior to printing. The inks were then allowed to air-dry to remove residual water after the centrifugation process prior to screen printing. Inks were printed manually with a rubber squeegee onto a Ryonet 200 mesh grid. Square films were printed for investigation.

IPL. The films were IPL processed with a Sinteron 2000 (Xenon Corporation) by applying 2.044 ms pulses of white light ranging from 240−1000 nm (Figure S2 of the Supporting Information). IPL processes were applied with 40 pulses at energy densities of 10.1, 12.8, 15.8, 19.2, 22.9, 26.8, 31.1 and 35.7 J cm^{-2}. A 15 s rest period, where no pulses were applied, was used between each set of 10 pulses to prevent cracking of the glass substrates. FTIR analysis was performed with samples processed at a constant energy density of 12.8 J cm^{-2}.

Characterization. A Bruker AXS D8 X-ray diffractometer using Ni-filtered Cu Kα radiation with a step size of 0.02° and a scan speed of 0.5 s/step was utilized for X-ray diffraction characterization of the crystal lattices. A FEI Nova NanoSEM 600 with an accelerating voltage of 2−3 kV and a working distance of 5−6 mm was used to study the morphology and extent of sintering of the deposits. Presence of organic molecules was observed with a PerkinElmer Spectrum BX FT-IR spectrometer through use of KBr pellets. The potassium bromide (KBr, ≥99%, Sigma-Aldrich) pellets were created by taking 15 mg of KBr and adding 2−5% of a given sample, by physical removal from substrate, and then pressing at 5 t for 10 min. All FTIR samples were collected with a varying amount of pulses at an energy density of 12.8 J cm^{-2} and normalized to account for weight variations. Sheet resistance measurements were carried out with a 4-point probe attached to a

DOI: 10.1021/acsami.5b03854
ACS Appl. Mater. Interfaces 2015, 7, 16478−16485

Keithley Model 2400 SourceMeter. For thickness measurements, a Technor Instruments alpha-Step 500 surface profiler was utilized.

CONCLUSION

Copper nitrate hydroxide was synthesized and successfully reduced into elemental copper, with the inclusion of fructose and glucose to decompose during the IPL process. The results shown help to understand further the reduction mechanism. Copper nitrate hydroxide was not found to transform into an intermediary copper oxide throughout the process. This is significant because less energy is required, which is favorable for its viability in future commercial applications.

As the copper nitrate hydroxide synthesized did convert to elemental copper only in the presence of the reducing agents, analysis of different organics, based on application, could be explored further. The lowest sheet resistance measured was 0.224 Ω/□. The sheet resistance of the films could be improved through the optimization of sugar ratios and IPL processing techniques. The deposition of inks through noncontact methods, such as inkjet printing, would further provide viability for future commercial applications.

ASSOCIATED CONTENT

Supporting Information

FTIR of $Cu_2(OH)_3NO_3$ with one, five and ten 12.8 J cm^{-2} pulses of IPL processing; intense pulsed light spectrum; sheet resistance of IPL processed fructose films with forty pulses at varying energy densities. The Supporting Information is available free of charge on the ACS Publications website at DOI: 10.1021/acsami.5b03854.

AUTHOR INFORMATION

Corresponding Author

*T. Druffel. E-mail: thad.druffel@louisville.edu.

Notes

The authors declare no competing financial interest.

ACKNOWLEDGMENTS

The authors acknowledge the Conn Center for Renewable Energy Research at the University of Louisville for their financial support. This research was supported in part by an award from the Kentucky Science and Technology Corporation under Contract No. KSTC-144-401-14-069.

REFERENCES

(1) Wünscher, S.; Abbel, R.; Perelaer, J.; Schubert, U. S. Progress of Alternative Sintering Approaches of Inkjet-Printed Metal Inks and their Application for Manufacturing of Flexible Electronic Devices. *J. Mater. Chem. C* **2014**, *2*, 10232−10261.

(2) Jeong, S.; Song, H. C.; Lee, W. W.; Lee, S. S.; Choi, Y.; Son, W.; Kim, E. D.; Paik, C. H.; Oh, S. H.; Ryu, B. H. Stable Aqueous Based Cu Nanoparticle Ink for Printing Well-Defined Highly Conductive Features on a Plastic Substrate. *Langmuir* **2011**, *27*, 3144−3149.

(3) Buffat, P.; Borel, J. P. Size Effect on the Melting Temperature of Gold Particles. *Phys. Rev. A: At., Mol., Opt. Phys.* **1976**, *13*, 2287−2298.

(4) Ryu, J.; Kim, H.-S.; Hahn, H. T. Reactive Sintering of Copper Nanoparticles Using Intense Pulsed Light for Printed Electronics. *J. Electron. Mater.* **2011**, *40*, 42−50.

(5) Hwang, H. J.; Chung, W. H.; Kim, H. S. In Situ Monitoring of Flash-Fight Sintering of Copper Nanoparticle Ink for Printed Electronics. *Nanotechnology* **2012**, *23*, 485205.

(6) Park, S.-H.; Chung, W.-H.; Kim, H.-S. Temperature Changes of Copper Nanoparticle Ink During Flash Light Sintering. *J. Mater. Process. Technol.* **2014**, *214*, 2730−2738.

(7) Pham, L. Q.; Sohn, J. H.; Kim, C. W.; Park, J. H.; Kang, H. S.; Lee, B. C.; Kang, Y. S. Copper Nanoparticles Incorporated with Conducting Polymer: Effects of Copper Concentration and Surfactants on the Stability and Conductivity. *J. Colloid Interface Sci.* **2012**, *365*, 103−109.

(8) Dharmadasa, R.; Jha, M.; Amos, D. A.; Druffel, T. Room Temperature Synthesis of a Copper Ink for the Intense Pulsed Light Sintering of Conductive Copper Films. *ACS Appl. Mater. Interfaces* **2013**, *5*, 13227−13234.

(9) Liu, Q.-m.; Zhou, D.-b.; Yamamoto, Y.; Ichino, R.; Okido, M. Preparation of Cu Nanoparticles with NaBH4 by Aqueous Reduction Method. *Trans. Nonferrous Met. Soc. China* **2012**, *22*, 117−123.

(10) Park, B. K.; Jeong, S.; Kim, D.; Moon, J.; Lim, S.; Kim, J. S. Synthesis and Size Control of Monodisperse Copper Nanoparticles by Polyol Method. *J. Colloid Interface Sci.* **2007**, *311*, 417−424.

(11) Biçer, M.; Şişman, İ. Controlled Synthesis of Copper Nano/Microstructures Using Ascorbic Acid in Aqueous CTAB Solution. *Powder Technol.* **2010**, *198*, 279−284.

(12) Deng, D.; Qi, T.; Cheng, Y.; Jin, Y.; Xiao, F. Copper Carboxylate with Different Carbon Chain Lengths as Metal−Organic Decomposition Ink. *J. Mater. Sci.: Mater. Electron.* **2014**, *25*, 390−397.

(13) Paquet, C.; James, R.; Kell, A. J.; Mozenson, O.; Ferrigno, J.; Lafrenière, S.; Malenfant, P. R. L. Photosintering and Electrical Performance of CuO Manoparticle Inks. *Org. Electron.* **2014**, *15*, 1836−1842.

(14) Hidmi, L.; Edwards, M. Role of Temperature and pH in $Cu(OH)_2$ Solubility. *Environ. Sci. Technol.* **1999**, *33*, 2607−2610.

(15) Wang, W.; Varghese, O. K.; Ruan, C.; Paulose, M.; Grimes, C. A. Synthesis of CuO and Cu_2O Crystalline Nanowires Using $Cu(OH)_2$ Nanowire Templates. *J. Mater. Res.* **2003**, *18*, 2756−2759.

(16) Li, Y.; Yang, X. Y.; Rooke, J.; Van Tendeloo, G.; Su, B. L. Ultralong $Cu(OH)_2$ and CuO Nanowire Bundles: PEG200-Directed Crystal Growth for Enhanced Photocatalytic Performance. *J. Colloid Interface Sci.* **2010**, *348*, 303−312.

(17) Park, S. H.; Kim, H. J. Unidirectionally Aligned Copper Hydroxide Crystalline Nanorods from Two-Dimensional Copper Hydroxy Nitrate. *J. Am. Chem. Soc.* **2004**, *126*, 14368−14369.

(18) Wang, X.-b.; Huang, L.-n A Novel One-Step Method to Synthesize Copper Nitrate Hydroxide Nanorings. *Trans. Nonferrous Met. Soc. China* **2009**, *19*, s480−s484.

(19) Zhang, L.; Lu, W.; Feng, Y.; Ni, J.; Lu, Y.; Shang, X. Facile Synthesis of Leaf-like Cu(OH)2 and Its Conversion into CuO with Nanopores. *Acta Phys. Chim. Sin.* **2008**, *24*, 2257−2262.

(20) Linder, G. G.; Atanasov, M.; Pebler, J. A Single-Crystal Study of the Magnetic Behavior and Exchange Coupling in $Cu_2(OH)_3NO_3$. *J. Solid State Chem.* **1995**, *116*, 1−7.

(21) Araki, T.; Sugahara, T.; Jiu, J.; Nagao, S.; Nogi, M.; Koga, H.; Uchida, H.; Shinozaki, K.; Suganuma, K. Cu Salt Ink Formulation for Printed Electronics using Photonic Sintering. *Langmuir* **2013**, *29*, 11192−11197.

(22) Arizaga, G.; Satyanarayana, K.; Wypych, F. Layered Hydroxide Salts: Synthesis, Properties and Potential Applications. *Solid State Ionics* **2007**, *178*, 1143−1162.

(23) Niu, H.; Yang, Q.; Tang, K. A New Route to Copper Nitrate Hydroxide Microcrystals. *Mater. Sci. Eng., B* **2006**, *135*, 172−175.

(24) Dharmadasa, R.; Dharmadasa, I. M.; Druffel, T. Intense Pulsed Light Sintering of Electrodeposited CdS Thin Films. *Adv. Eng. Mater.* **2014**, *16*, 1351−1361.

(25) Henrist, C.; Traina, K.; Hubert, C.; Toussaint, G.; Rulmont, A.; Cloots, R. Study of the Morphology of Copper Hydroxynitrate Nanoplatelets Obtained by Controlled Double Jet Precipitation and Urea Hydrolysis. *J. Cryst. Growth* **2003**, *254*, 176−187.

(26) Witowski, J.; Jorres, A. Glucose Degradation Products: Relationship with Cell Damage. *Peritoneal Dial. Int.* **2000**, *20*, S31−S36.

(27) Soininen, P. J.; Elers, K. E.; Saanila, V.; Kaipio, S.; Sajavaara, T.; Haukka, S. Reduction of Copper Oxide Film to Elemental Copper. *J. Electrochem. Soc.* **2005**, *152*, G122.

DOI: 10.1021/acsami.5b03854
ACS Appl. Mater. Interfaces 2015, 7, 16478−16485

(28) Lee, J. W.; Thomas, L. C.; Schmidt, S. J. Investigation of the Heating Rate Dependency Associated with the Loss of Crystalline Structure in Sucrose, Glucose, and Fructose Using a Thermal Analysis Approach (Part I). *J. Agric. Food Chem.* **2011**, *59*, 684−701.
(29) Setzer, W. N. A DFT Analysis of Thermal Decomposition Reactions Important to Natural Products. *Nat. Prod. Commun.* **2010**, *5*, 993−998.
(30) Jha, M.; Dharmadasa, R.; Draper, G. L.; Sherehiy, A.; Sumanasekera, G.; Amos, D.; Druffel, T. Solution Phase Synthesis and Intense Pulsed Light Sintering and Reduction of a Copper Oxide Ink with an Encapsulating Nickel Oxide Barrier. *Nanotechnology* **2015**, *26*, 175601.

DOI: 10.1021/acsami.5b03854
ACS Appl. Mater. Interfaces 2015, 7, 16478−16485